

## Article

# ZrO<sub>2</sub> Nanoparticles and Poly(diallyldimethylammonium chloride)-Doped Graphene Oxide Aerogel-Coated Stainless-Steel Mesh for the Effective Adsorption of Organophosphorus Pesticides

Xiudan Hou <sup>1</sup>, Rong Ding <sup>1</sup>, Shihai Yan <sup>2</sup>, Haiyan Zhao <sup>1</sup>, Qingli Yang <sup>1</sup> and Wei Wu <sup>1,\*</sup> 

<sup>1</sup> College of Food Science and Engineering, Qingdao Agricultural University, Qingdao 266109, China; qdxdhou@qau.edu.cn (X.H.); dingr1025@163.com (R.D.); xinyuyuan@163.com (H.Z.); yql@qau.edu.cn (Q.Y.)

<sup>2</sup> College of Chemistry and Pharmaceutical Sciences, Qingdao Agricultural University, Qingdao 266109, China; shyan@qau.edu.cn

\* Correspondence: wuweiou@126.com; Tel.: +86-532-86080771; Fax: +86-532-86080221

**Abstract:** A novel sorbent based on the ZrO<sub>2</sub> nanoparticles and poly(diallyldimethylammonium chloride)-modified graphene oxide aerogel-grafted stainless steel mesh (ZrO<sub>2</sub>/PDDA-GOA-SSM) was used for the extraction and detection of organophosphorus pesticides (OPPs). Firstly, the PDDA and GO composite was grafted onto the surface of SSM and then freeze-dried to obtain the aerogel, which efficiently reduced the accumulation of graphene nanosheets. It integrated the advanced properties of GOA with a thin coating and the three-dimensional structural geometry of SSM. The modification of ZrO<sub>2</sub> nanoparticles brought a selective adsorption for OPPs due to the combination of the phosphate group as a Lewis base and ZrO<sub>2</sub> nanoparticles with the Lewis acid site. The ZrO<sub>2</sub>/PDDA-GOA-SSM was packed into the solid-phase extraction (SPE) cartridge to extract OPPs. According to the investigation of different factors, the extraction recovery was mainly affected by the hydrophilic-hydrophobic properties of analytes. Effective extraction and elution parameters such as sample volume, sample pH, rate of sample loading, eluent, and eluent volume, were also investigated and discussed. Under the optimal conditions, the linearity of phoxim and fenitrothion was in the range of 1.0–200 µg L<sup>-1</sup>, and the linearity of temephos was in the range of 2.5–200 µg L<sup>-1</sup>. The limits of detection were ranged from 0.2 to 1.0 µg L<sup>-1</sup>. This established method was successfully applied to detect OPPs in two vegetables. There was no OPP detected in real samples, and results showed that the matrix effects were in the range of 46.5%–90.1%. This indicates that the ZrO<sub>2</sub>/PDDA-GOA-SSM-SPE-HPLC method could effectively extract and detect OPPs in vegetables.

**Keywords:** graphene aerogel; ZrO<sub>2</sub>; solid-phase extraction; organophosphorus pesticides



**Citation:** Hou, X.; Ding, R.; Yan, S.; Zhao, H.; Yang, Q.; Wu, W. ZrO<sub>2</sub> Nanoparticles and Poly(diallyldimethylammonium chloride)-Doped Graphene Oxide Aerogel-Coated Stainless-Steel Mesh for the Effective Adsorption of Organophosphorus Pesticides. *Foods* **2021**, *10*, 1616. <https://doi.org/10.3390/foods10071616>

Academic Editor: Evaristo Ballesteros

Received: 19 May 2021

Accepted: 28 June 2021

Published: 13 July 2021

**Publisher's Note:** MDPI stays neutral with regard to jurisdictional claims in published maps and institutional affiliations.



**Copyright:** © 2021 by the authors. Licensee MDPI, Basel, Switzerland. This article is an open access article distributed under the terms and conditions of the Creative Commons Attribution (CC BY) license (<https://creativecommons.org/licenses/by/4.0/>).

## 1. Introduction

Pesticide residue is an importantly concerning aspect of food safety. Nowadays, the population of food poisoning caused by pesticides occupies one-third of the total number of people of food poisoning, among which organophosphorus pesticides (OPPs) take the first place. OPPs, as a class of agricultural chemicals, are mainly used to prevent the invasion of insects. However, excess of OPPs remain in the surface and body of agricultural products, infiltrate into the environmental samples, and furthermore, enter into the human body, which can cause headache, dyspnea, and dysphoria symptoms [1,2]. The long-term consumption of these pesticides can lead to cancer and even death [3]. China and other countries have stipulated that the maximum residue limit of most OPPs should not be higher than 0.2 mg kg<sup>-1</sup> or 0.5 mg kg<sup>-1</sup> [4]. Therefore, it is important to detect and monitor OPPs in food in order to guarantee the food safety.

Due to the complexity of matrices in food samples, the diversity of ingredients, and trace residue level, it is exceedingly difficult to detect OPPs directly making use of an instrument. Generally, a suitable sample pretreatment method is chosen to separate and enrich target OPPs prior to using the instrument in order to improve the sensitivity and accuracy. Traditional extraction methods including liquid–liquid extraction and solid-phase extraction have some disadvantages such as being highly organic solvent consuming and time consuming, etc. In recent years, many new material-based extraction methods have been introduced to detect OPPs, e.g., dispersive liquid–liquid microextraction [5], hollow-fiber liquid-phase microextraction [6], dispersive micro-solid phase extraction [7], magnetic solid-phase extraction [1], ultrasound-assisted emulsification liquid-phase microextraction [8], fiber solid-phase microextraction [9], etc., which can shorten the extraction time and minimize the solvent consumption. Nowadays, the studied extraction materials mainly include metal organic frameworks [10,11], covalent organic frameworks [12], layered double hydroxides [13], molecularly imprinted polymers [14], graphitic carbon nitride [15,16], and ionic liquid [17–19].

The stainless-steel mesh-based sorptive extraction was introduced as a new extraction method [20]. A large amount of adsorption materials can be coated onto the surface of meshes to greatly increase the contact surface area, and the extraction equilibrium is relatively faster.

Graphene aerogel (GA) has attracted more and more attention in different fields since its emergence in 2013 owing to the super large specific surface area, excellent mechanical properties, high porosity, and low density [21–23]. As a desirable sorbent, porous and amphiphilic GA was designed and prepared for the adsorption and preconcentration of environmental pollutants [24–27]. Although the 3D frame structure of GA can provide many adsorption sites, it has the disadvantage of a single structure with the poor adsorption selectivity for OPPs. Therefore, in order to achieve high-efficiency enrichment of trace OPPs in complex food samples, it is necessary to prepare functionalized GA to improve the extraction performance. Furthermore, it can be realized through the framework structure, oxygen-containing groups, and the interaction of the carbon skeleton of graphene oxide aerogel (GOA). However, it remains to be solved that GA not only possesses good mechanical strength, but also offers excellent extraction performance for OPPs. Some polymers are capable of elevating the mechanical features of GA [28,29]. For example, Bai et al., fabricated a porous GOA using polyethyleneimine as the cross-linking agent to avoid the collapse of the structure, which was successfully used to extract thorium (IV) from three lanthanides (III) elements [30]. Poly(diallyldimethylammonium chloride) (PDDA) was regarded as a cationic polyelectrolyte due to the abundance of positively charged quaternary ammonium groups, which were widely used in many fields [31–33]. PDDA could be introduced to prevent the irreversible agglomerate of graphene nanosheets and also enhance the mechanical stability to avoid the collapse of the aerogel structure.

Zirconia ( $\text{ZrO}_2$ ), as an inorganic oxide, exhibited excellent properties of high specific surface area, chemical inertness, thermal stability, and lack of toxicity [34]. It has been reported that  $\text{ZrO}_2$  possesses a strong affinity for the phosphoric group, and the phosphate group as a Lewis base could strongly interact with the Lewis acid site on the surface of  $\text{ZrO}_2$  to form coordination bonds, which makes  $\text{ZrO}_2$  as a selective sorbent for the detection of OPPs [35].  $\text{ZrO}_2$ -based sorbents were used for the selective determination of OPPs in real samples [36–38]. Individual  $\text{ZrO}_2$  nanoparticles were easy to aggregate. In order to expose more adsorption sites, nanosheet-structured graphene as a desirable material could be utilized to improve the dispersity of  $\text{ZrO}_2$  nanoparticles.

This work prepared a  $\text{ZrO}_2$  nanoparticles and PDDA-modified GOA-grafted stainless-steel mesh ( $\text{ZrO}_2$ /PDDA-GOA-SSM) as the sorbent for the extraction of OPPs. The material enhanced with PDDA exhibited higher stability. This sorbent device integrated the advantages of the sorptive extraction and the adsorption property of GOA. Various surface analysis techniques were used to characterize the morphology, structure, and composition of  $\text{ZrO}_2$ /PDDA-GOA-SSM. A SPE column was packed with  $\text{ZrO}_2$ /PDDA-GOA-SSM to

extract OPPs. The applicability of the established  $ZrO_2$ /PDDA-GOA-SSM-SPE-HPLC method was also evaluated.

## 2. Materials and Methods

### 2.1. Materials and Reagents

The stainless-steel mesh (SUS304, pore 74  $\mu\text{m}$ ,  $\Phi$  50  $\mu\text{m}$ ) was purchased from Leiko Metal Products Co. LTD (Changzhou, China). Graphite powder, phoxim (99%), temephos (99%), fenitrothion (99%), 3-aminopropyltriethoxysilane (APTES), PDDA (MW = 200,000–300,000), N-hydroxy succinimide (NHS), and N-(3-dimethylaminopropyl)-N-ethyl-carbodiimide (EDC) were all obtained from Aladdin Chemical Reagent Co. (Shanghai, China). Zirconyl chloride octahydrate ( $ZrOCl_2 \cdot 8H_2O$ ) was obtained from Macklin Biochemical Co. Ltd. (Shanghai, China). The SPE empty column (3 mL), polyethylene sieve plates (20  $\mu\text{m}$  pore size), and commercial sorbents (C18, Carb, SAX, Florisil,  $NH_2$ ) were all supplied by Shenzhen Biocomma Biotech Co. (Shenzhen, China).

### 2.2. Apparatus

The SPE procedure was carried out on an SPE80 vacuum manifold equipped with 8-port model and a peristaltic pump (Jinan, China). The chromatographic separation and analysis of OPPs was performed on an Ultimate 3000 modular HPLC system with an automatic sampler (20  $\mu\text{L}$  injection loop) and a UV-vis detector (Thermo Fisher Scientific, Waltham, MA, USA). A C18 column (Hypersil ODS2, 250 mm length  $\times$  4.6 mm i.d., 5  $\mu\text{m}$ ) was used for the separation of analytes. The mobile phase was composed of different proportions of methanol and water, the gradient elution was: 0–12 min, 73% methanol; 12–13 min, 73%–78% methanol. Two organic or water membranes (0.45  $\mu\text{m}$ ) were used to filter these mobile phases. The oven temperature was 25  $^\circ\text{C}$ . The flow rate of mobile phase was set at 1.0  $\text{mL min}^{-1}$ . The detection wavelength was 254 nm.

The synthesized materials were characterized using a series of instruments and equipment. A scanning electron microscope (SEM, JSM-6701F, JEOL, Tokyo, Japan) was used to observe the surface morphology. An IFS120HR Fourier transform infrared (FT-IR, Bruker, Karlsruhe, Germany) spectrometer (Thermo Fisher Scientific, Waltham, MA, USA) and an X-ray photoelectron spectrometer (XPS, ESCALAB 250Xi, Thermo Fisher Scientific, Waltham, MA, USA) were used to verify the component. A thermal gravimetric analyzer (TGA, STA449C, Netzsch, Selbu, Germany) was used to characterize the thermal stability. A BET analyzer (ASAP 2010, Micromeritics, Norcross, GA, USA) was used to obtain the surface area.

### 2.3. Preparation of Adsorption Materials

GO was firstly synthesized according to the modified Hummer's method, which was described in the previous work [39]. Firstly, the SSM ( $\Phi$  8 mm) was immersed into the diluted hydrochloric acid to be etched, and after it was dried, it was put in APTES for 12 h to complete the modification of amino. Then, the obtained SSM was placed into a 5 mL centrifuge tube in addition to 4 mL of GO suspension (0.1 wt%), 0.001 g PDDA, 0.001 g EDC, and 0.001 g NHS, reacting for 2 h at 70  $^\circ\text{C}$ , which was then repeated 3 times to attain a coating with a desirable thickness. Furthermore,  $ZrO_2$  nanoparticles were deposited onto the surface of GO-grafted SSM through the reaction of  $ZrOCl_2 \cdot 8H_2O$  in ammonia water, which was added into a reaction kettle for 12 h at 180  $^\circ\text{C}$ . Finally, it was transferred to a freeze dryer (20 Pa,  $-50$   $^\circ\text{C}$ ), and after 10 h, the  $ZrO_2$ /PDDA-GOA-SSM was obtained. Figure 1 illustrates a sequence of preparation steps of the preparation of  $ZrO_2$ /PDDA-GOA-SSM.

The commercial sorbents including C18,  $-NH_2$ , SAX, Carb, and Florisil, were removed from their original SPE column, and 50 mg of each of them were refilled into the new SPE column, respectively.

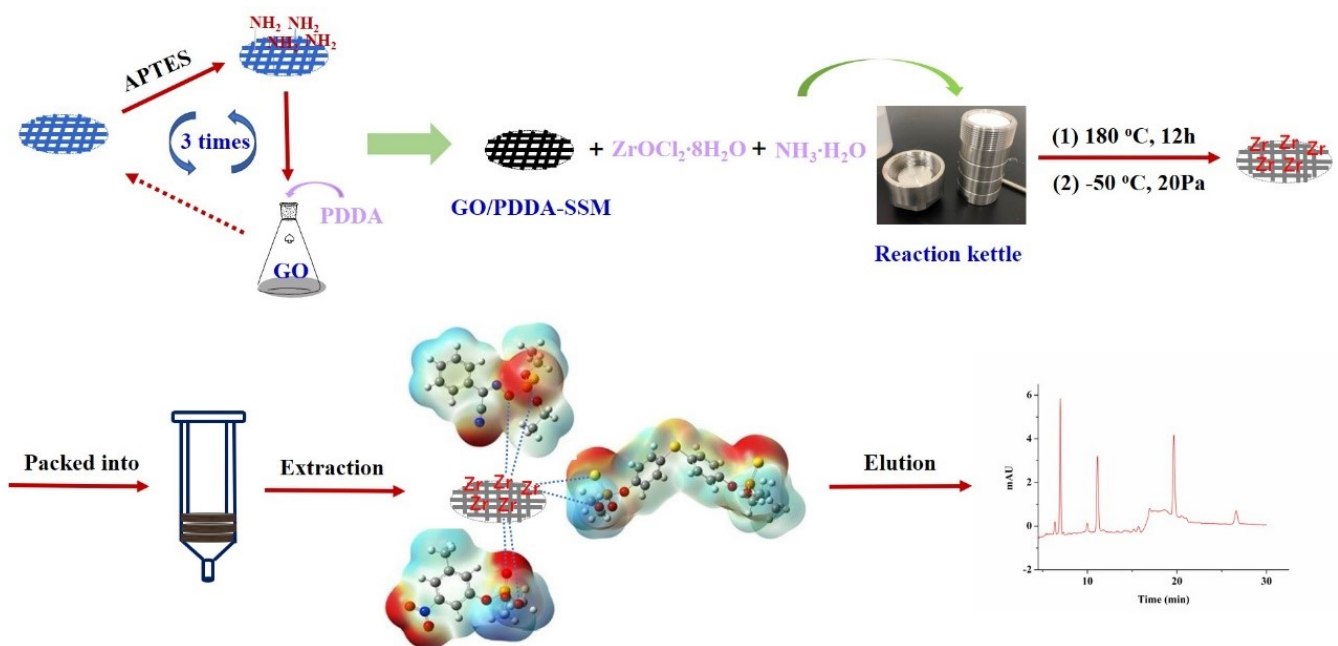


**Figure 1.** Preparation of the ZrO<sub>2</sub>/PDDA-GOA-modified SSM and the response signal.

#### 2.4. Sample Preparation and Extraction Procedure

Two vegetables (chives and pak choi) were bought from the local market (Qingdao, China). Firstly, they were twisted into powder in a high-speed pulverizer. One gram of the powder was put into an ethanol/water (10 mL, *v/v*, 70:30) and shaken for 3 h at 55 °C. After that, the mixture was centrifuged to remove the sample residue and retain the extractant. Then, the extractant was evaporated under the N<sub>2</sub> stream. Finally, the residue was reconstituted with 20 mL of ultrapure water waiting for the extraction. In the study of relative recoveries, different volumes (2 µL, 4 µL, 10 µL) of the OPP standard solution (200 µg L<sup>-1</sup>) were added into the above 10 mL of mixture with ethanol/water and the sample.

The extraction procedure was performed on an SPE semi-automatic extraction apparatus. Three pieces of ZrO<sub>2</sub>/PDDA-GOA-SSM were filled into an empty plastic column, which was held with two sieve plates at each end of the cartridge. The prepared SPE column was preconditioned with 10 mL of water/acetonitrile (*v/v*, 1:1). A 20 mL aqueous sample containing three OPPs at the concentration of 200 µg L<sup>-1</sup> was loaded onto the ZrO<sub>2</sub>/PDDA-GOA-SSM sorbent at a flow rate of 1.5 mL min<sup>-1</sup>. Then, 0.5 mL of water was used to wash the sorbent to remove other impurities. After drying for 5 min in air, the eluent (1.0 mL of acetonitrile) was used to elute the reserved OPPs on the ZrO<sub>2</sub>/PDDA-GOA-SSM at a flow rate of 0.8 mL min<sup>-1</sup>. Finally, the obtained extract was directly injected into the HPLC-UV system. Three replicate measurements were carried out to obtain the average value.

#### 2.5. Adsorption Experiment

In the static-state adsorption experiment, one piece of ZrO<sub>2</sub>/PDDA-GOA-SSM was put into a 1.5 mL centrifuge tube with 1.0 mL of OPPs standards at different concentrations in the range of 5–30 µg mL<sup>-1</sup>. The adsorption time was 30 min and the process was carried out at room temperature. The adsorption capacity of ZrO<sub>2</sub>/PDDA-GOA-SSM towards OPPs was calculated and evaluated through the comparison of ZrO<sub>2</sub>/PDDA-GOA-SSM towards different OPPs. The calculation equation was as follows:

$$q = (C_i - C_f) \times V_s \quad (1)$$



where  $q$  ( $\mu\text{g}$ ) is the adsorption amount of OPP on one piece of  $\text{ZrO}_2/\text{PDDA-GOA-SSM}$ ;  $V_s$  is the volume of sample; and  $C_i$  and  $C_f$  ( $\mu\text{g mL}^{-1}$ ) are the initial and final concentrations of OPP, respectively.

The adsorption behavior of each OPP on the surface of  $\text{ZrO}_2/\text{PDDA-GOA-SSM}$  was fitted by the Langmuir and Freundlich isotherm models, and their equations are as follows:

$$\frac{C_e}{q_e} = \frac{C_e}{q_{max}} + \frac{1}{K_L q_{max}} \quad (2)$$

$$q_e = K_F C_e^{1/n} \quad (3)$$

where  $q_e$  ( $\mu\text{g}$ ) and  $q_{max}$  ( $\mu\text{g}$ ) are the adsorption amount of OPP at the equilibrium and the maximum amount to form the single layer, respectively;  $K_L$  ( $\text{mL g } \mu\text{g}^{-1}$ ) and  $K_F$  [ $\mu\text{g (mL } \mu\text{g}^{-1})$ ] are constants to reflect the adsorption capacity;  $C_e$  ( $\mu\text{g mL}^{-1}$ ) is the concentration of OPP at the equilibrium; and  $n$  reflects the adsorption affinity of  $\text{ZrO}_2/\text{PDDA-GOA-SSM}$  for OPPs.

A dimensionless constant ( $R_L$ ) called the separation factor or equilibrium parameter was defined as follows:

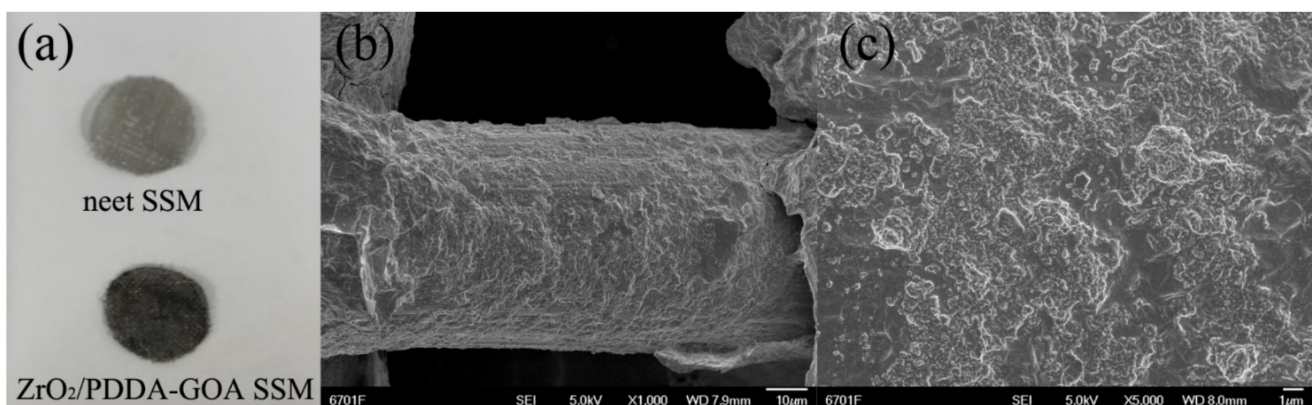
$$R_L = \frac{1}{1 + C_0 K_L}$$

where  $C_0$  is the highest initial concentration of OPPs.  $R_L$  is a measure of the adsorption nature:  $R_L = 0$  (irreversible),  $0 < R_L < 1$  (favorable),  $R_L = 1$  (linear), and  $R_L > 1$  (unfavorable).

### 3. Results

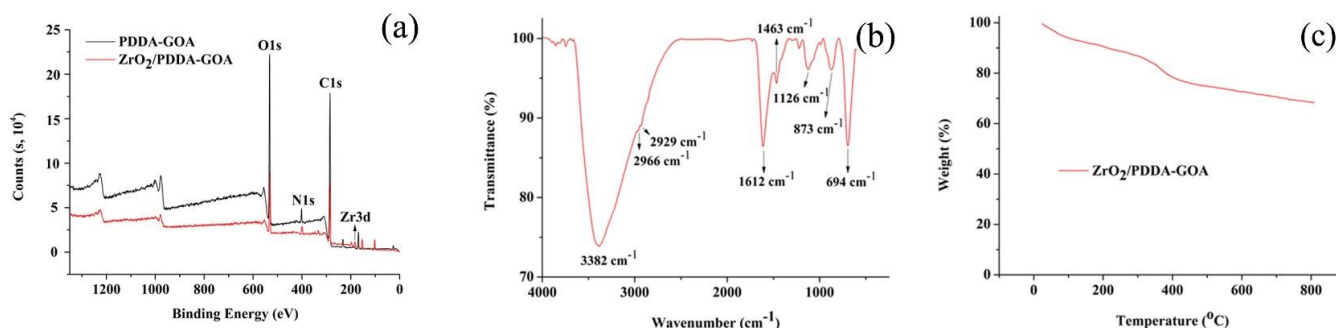
#### 3.1. Characterization of the Sorbent

Figure 2a showed the photographs of the neat SSM and  $\text{ZrO}_2/\text{PDDA-GOA}$ -modified SSMs. Compared with the bare SSM, it can be obviously observed that the GOA composite was successfully covered onto the surface of SSM. The surface morphology of  $\text{ZrO}_2/\text{PDDA-GOA}$ -modified SSM was also investigated through the SEM characterization. Figure 2b showed the skeleton structure of SSM and the connection of stainless-steel wire to form the mesh structure. SEM images confirmed that the  $\text{ZrO}_2$  nanoparticle-modified graphene sheets were completely and uniformly coated onto the surface of every stainless-steel wire of SSM. Figure S1 exhibits the SEM images of the etched SSM, PDDA-GOA-SSM, and  $\text{ZrO}_2/\text{PDDA-GOA-SSM}$ . Compared to the etched SSM ( $\Phi$  50  $\mu\text{m}$ ), the surface of  $\text{ZrO}_2/\text{PDDA-GOA-SSM}$  was rougher and more rugged, and the thickness of  $\text{ZrO}_2/\text{PDDA-GOA}$  was approximately 5  $\mu\text{m}$ . The BET surface area of the whole  $\text{ZrO}_2/\text{PDDA-GOA}$ -coated SSM was characterized as 58.47  $\text{m}^2 \text{g}^{-1}$ , which was higher than the surface area of 37.29  $\text{m}^2 \text{g}^{-1}$  of  $\text{ZrO}_2/\text{PDDA-GO}$ -coated SSM.



**Figure 2.** Photographs of the bare SSM and  $\text{ZrO}_2/\text{PDDA-GOA}$ -modified SSM (a) and SEM images of  $\text{ZrO}_2/\text{PDDA-GOA}$ -modified SSM with different magnifications (b,c).

The XPS analysis was performed to evaluate the successful synthesis of  $\text{ZrO}_2/\text{PDDA-GOA}$ . As shown in Figure 3a, the C, O, and N elements all appeared in PDDA-GOA and  $\text{ZrO}_2/\text{PDDA-GOA}$ . Besides, the peak of 183 eV ( $\text{Zr}3d$ ) appeared in  $\text{ZrO}_2/\text{PDDA-GOA}$ , which verified the successful modification of  $\text{ZrO}_2$ .



**Figure 3.** Characterization of extraction materials: XPS analysis (a), FT-IR spectrum (b), and TGA analysis (c).

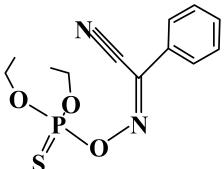
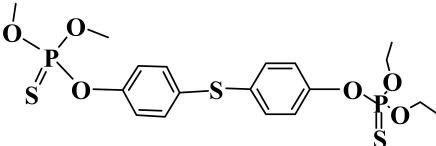
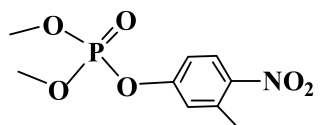
The functional groups of  $\text{ZrO}_2/\text{PDDA-GOA}$  were identified through the FT-IR spectroscopy. As can be seen in Figure 3b, the broad and strong peak observed at  $3382\text{ cm}^{-1}$  was attributed to the O-H and N-H stretching vibrations from GOA and PDDA, respectively. The peaks at  $2966\text{ cm}^{-1}$ ,  $2929\text{ cm}^{-1}$ , and  $1463\text{ cm}^{-1}$  were referred to the stretching vibrations of saturated and unsaturated C-H bonds, and their bending vibration, respectively. The peak at  $1612\text{ cm}^{-1}$  corresponded to the C=O stretching vibration of -COOH in GOA. The appearance of peak  $1126\text{ cm}^{-1}$  was attributed to the stretching vibration of Zr-O-H groups. Characteristic peaks at  $694\text{ cm}^{-1}$  and  $873\text{ cm}^{-1}$  corresponded to the Zr-O bond as longitudinal and transverse modes, respectively. Meanwhile, the bending vibration of the benzene ring in GOA was in the range of  $800\text{--}900\text{ cm}^{-1}$ , so the peak at  $873\text{ cm}^{-1}$  was relatively wider. The FT-IR spectrum further verified the successful preparation of the  $\text{ZrO}_2/\text{PDDA-GOA}$  composite.

The thermal stability of  $\text{ZrO}_2/\text{PDDA-GOA}$  was analyzed and assessed by thermogravimetric analysis (Figure 3c). The weight loss appeared below  $100\text{ °C}$  and in the range of  $100\text{--}300\text{ °C}$ , which was attributed to the loss of physisorbed and chemisorbed water, respectively. The weight loss ranging from  $300\text{ °C}$  to  $400\text{ °C}$ , and above  $400\text{ °C}$ , was ascribed to the thermal decomposition of PDDA. The TGA curve indicated that the weight loss of the composite was mainly due to the water and a small amount of polymer, and the loading of  $\text{ZrO}_2$  on the surface of GOA was relatively stable.

### 3.2. Interaction Energy

The theoretical interaction energies between  $\text{ZrO}_2$  and three OPPs were calculated with the Gaussian 09 software based on the density functional theory. Through the repeat adjustment and optimization of acting sites and interaction models between  $\text{ZrO}_2$  and three OPPs, the interaction energies were calculated. In the calculated process, the  $\pi\text{--}\pi$  interaction, hydrogen bonding, and coordination bonding were all taken into consideration. As shown in Table 1, binding energies ( $\Delta\text{HF}$ ) of phoxim, temephos, and fenitrothion on the  $\text{ZrO}_2$  nanoparticle were  $-40.89$ ,  $-34.03$ , and  $-46.93\text{ kcal mol}^{-1}$ , respectively. The changes of Gibbs free energy ( $\Delta\text{G}$ ) were  $-26.04$ ,  $-20.25$ , and  $-32.40\text{ kcal mol}^{-1}$ , respectively. The coordination interaction between Zr and O was stronger than that of Zr and S. Therefore, compared with other two OPPs, fenitrothion possessing the P=O group showed higher binding energy with  $\text{ZrO}_2$  nanoparticles. The negative value of  $\Delta\text{G}$  demonstrated that OPPs would all spontaneously combine with  $\text{ZrO}_2$  nanoparticles.

**Table 1.** Interaction energies of three OPPs on the ZrO<sub>2</sub> nanoparticle and octanol-water partition coefficient (log *K<sub>ow</sub>*) of OPPs.

Analyte	Structure	$\Delta H_F$ (kcal mol <sup>-1</sup> )	$\Delta G$ (kcal mol <sup>-1</sup> )	Log <i>K<sub>ow</sub></i>
Phoxin		-40.9	-26.0	4.4
Temephos		-34.0	-20.3	5.9
Fenitrothion		-46.9	-32.4	3.3

### 3.3. Optimization of the Extraction Procedure

In this experiment, three pieces of ZrO<sub>2</sub>/PDDA-GOA-SSM were selected to be packed into the SPE column. Using less pieces of mesh could bring about a relatively low adsorption amount, while using more pieces of mesh could lead to the blocking of sieve plates and decrease the flow rate. Other experimental conditions including volume of the sample, sample pH, the rate of sample loading, the eluent, and volume of the eluent, were optimized to increase the extraction efficiency. In the optimization experiments, the deionized water was used to dilute the mother liquor of analytes to 200 µg L<sup>-1</sup>.

#### 3.3.1. Extraction Conditions

The volume of the sample should be optimized as a higher volume to improve the enrichment factor. However, due to the finite amount of extraction material and finite adsorption sites, the adsorption amount for analytes was limited. Different volumes of sample were loaded from 5 mL to 60 mL measured by the ZrO<sub>2</sub>/PDDA-GOA-SSM-SPE-HPLC-UV method. Figure 4a exhibits that the extraction recoveries remained almost unchanged until 20 mL of the sample, and after that, the extraction efficiency gradually decreased. Thus, 20 mL was considered as the optimum sample volume.

The effect of the sample loading rate on the extraction efficiency was two-sided. In general, a high rate of sample loading would decrease the operation time. However, due to the insufficient contact between analytes and the sorbent, analytes could run off at a high rate and a shorter time. On the contrary, a lower rate would cause the “back-extraction” appearance of analytes between the sorbent and the sample solution. As shown in Figure 4b, extraction recoveries of three OPPs first rose and then went down. Hence, 1.0 mL min<sup>-1</sup> as the sample loading rate was selected.

Sample pH affected the existing state of analytes and the charge form of sorbents. A change of sample pH would bring about the gain or loss of protons. The investigated result is shown in Figure 4c. This indicates that OPPs in the molecular form would easily overflow from the sample matrix in the original solution. Hence, the pH value of the sample remained unchanged in the following experiment.

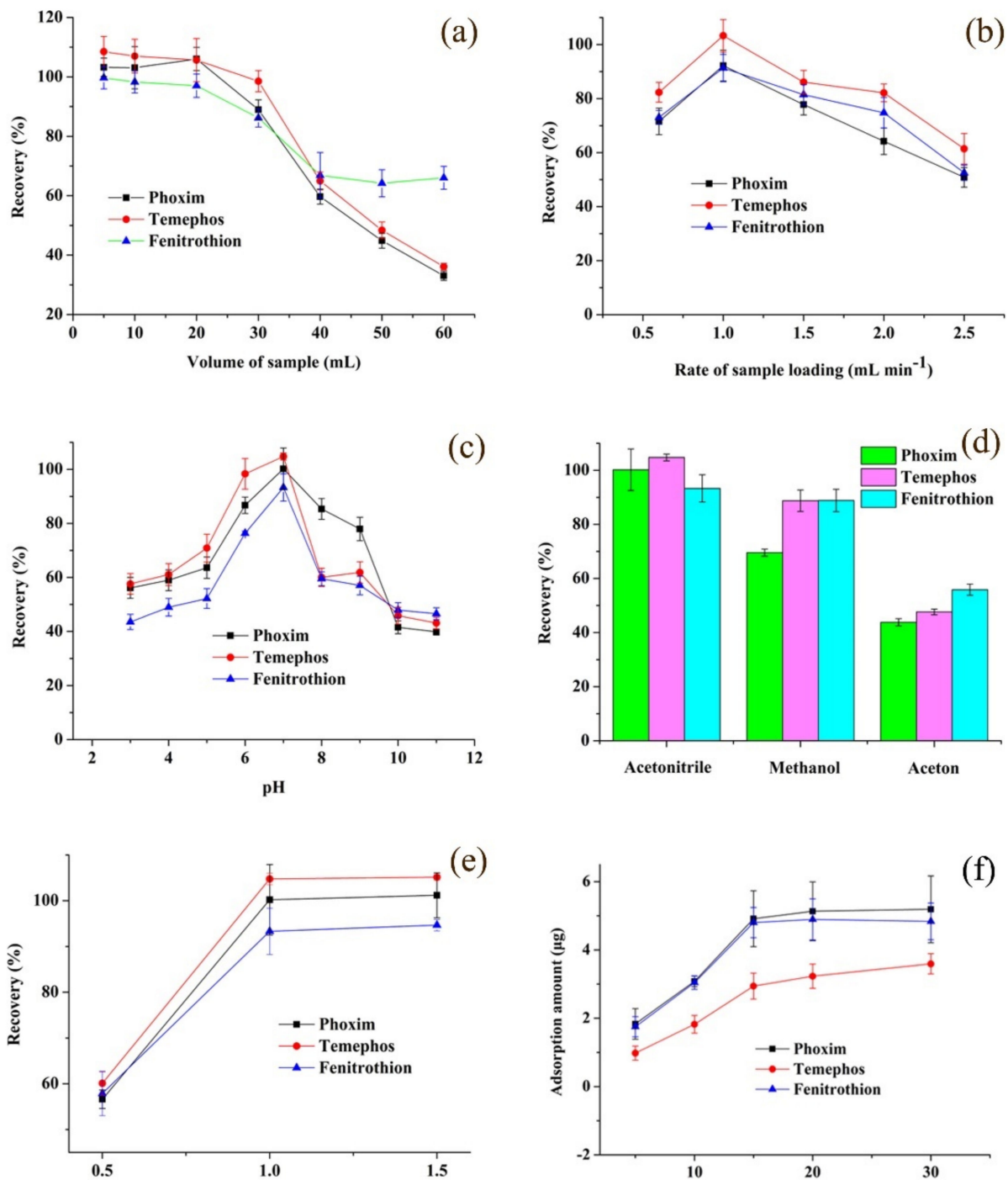


**Figure 4.** Effect of extraction and desorption conditions on the extraction performance: volume of sample (a), rate of sample loading (b), sample pH (c), type of eluent (d), volume of eluent (e); as well as the adsorption capacity-concentration profiles of analytes (f).

### 3.3.2. Desorption Conditions

A suitable eluent was an effective parameter to increase the extraction efficiency. A desirable desorption solvent must sufficiently elute all analytes from the surface of extraction materials. Several commonly used solvents including acetonitrile, methanol, and acetone were investigated. Figure 4d shows that acetonitrile as the eluent exhibited the highest extraction efficiency among three types of eluent. Thus, acetonitrile was used as the eluent of OPPs desorbed from the ZrO<sub>2</sub>/PDDA-GOA-SSM.



In the desorption process, when the eluent flowed past the sorbent, a minimum of eluent volume should be used in order to save organic solvent under the complete desorption of analytes. As shown in Figure 4e, acetonitrile samples in the range of 0.5–1.5 mL were investigated, respectively. The result presented that 1.0 mL of acetonitrile would elute analytes sufficiently. Therefore, 1.0 mL of acetonitrile was used to elute OPPs adsorbed in ZrO<sub>2</sub>/PDDA-GOA-SSM.

### 3.4. Extraction Performance and Extraction Mechanism

The ZrO<sub>2</sub>/PDDA-GO-coated SSM was also directly dispersed into the sample solution to extract OPPs, but it was found that several modified materials would fall down from the surface of SSM with the prolonging of operation time. Thus, the SPE method was used to prevent the problem, in which ZrO<sub>2</sub>/PDDA-GO-coated SSM was packed into the SPE column with two sieve plates at the ends.

The extraction performance of commercial sorbents (C18, -NH<sub>2</sub>, SAX, Carb, and Florisil) and prepared materials (APTES-SSM, PDDA-GO-SSM, PDDA-GOA-SSM, and ZrO<sub>2</sub>/PDDA-GO-SSM) for the extraction of three OPPs are exhibited in Figure 5. Compared with single APTES-modified SSM, extraction recoveries of the prepared ZrO<sub>2</sub>/PDDA-GO- and ZrO<sub>2</sub>/PDDA-GOA-modified SSM were obviously improved. Through the freeze-drying of GO, the forming of GA brought the increase of extraction efficiency. Compared with various commercial sorbents, it was observed that the extraction efficiencies of ZrO<sub>2</sub>/PDDA-GOA-SSM for the three OPPs were obviously increased, which indicated the superiority of the prepared composite.

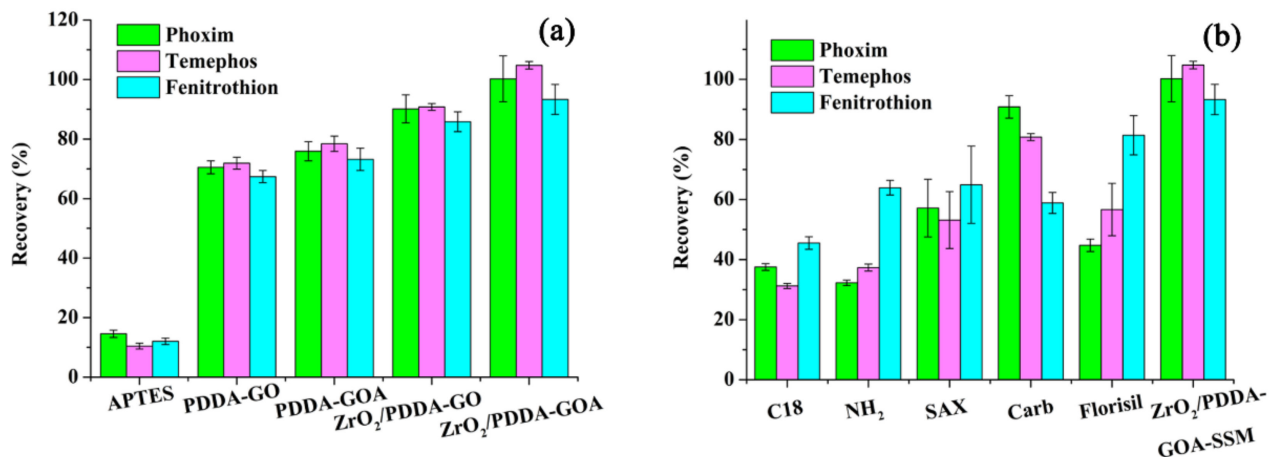


**Figure 5.** Comparison of extraction performance of different sorbents for analytes: (a) different prepared sorbent; (b) commercial sorbents.

To further evaluate the adsorption capacity of ZrO<sub>2</sub>/PDDA-GOA-SSM, the static-state binding experiment was investigated at different concentrations of OPPs. Figure 4f shows the adsorption capacity-concentration profiles of analytes. When the initial concentration of OPPs increased, the adsorption amount of each OPP also increased, which presented a saturation adsorption at the initial concentration of 15  $\mu\text{g mL}^{-1}$ , and then reached a plateau from 15  $\mu\text{g mL}^{-1}$  to 30  $\mu\text{g mL}^{-1}$ . The relationship between the adsorption amount and initial concentration was fitted through two most common theoretical adsorption models (Langmuir and Freundlich isotherms). Equations (2) and (3) were used to calculate the adsorption parameters, which are listed in Table S1. They exhibited higher correlation coefficients than Freundlich model, which indicates that the adsorption process of three OPPs onto the surface of ZrO<sub>2</sub>/PDDA-GOA-SSM was closer to the Langmuir model. Furthermore, it demonstrated that the target OPPs were adsorbed onto the surface of ZrO<sub>2</sub>/PDDA-GOA-SSM in the monolayer coverage. In the Langmuir model, RL values,

as the equilibrium parameter, were 0.3144, 0.5082, and 0.3257 for phoxim, temephos, and fenitrothion, respectively. This indicates that the adsorption was favorable.

Relative factors affecting the extraction recovery are all exhibited in Figure 6. The adsorption capacity of sorbent for analytes and the hydrophilic-hydrophobic property of analytes (octanol-water partitioning coefficient,  $\text{Log}K_{ow}$ ) co-determine the extraction recovery. Variation tendencies of theoretical adsorption energy and the adsorption amount were almost consistent, and the adsorption capacity was phoxim > temephos > fenitrothion. This indicates that the extraction recovery was mainly affected by the hydrophilic-hydrophobic property of analytes.

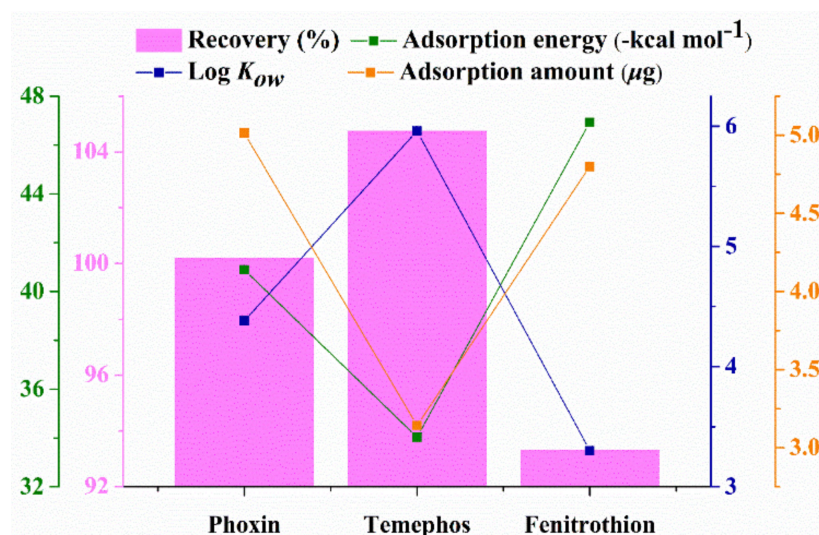


Figure 6. The variation tendency of different affecting factor.

### 3.5. Evaluation of the Method

Under the optimized experimental conditions, the analytical performance of the established  $\text{ZrO}_2/\text{PDDA-GOA-SSM-SPE-HPLC-UV}$  method was evaluated, which included the linear range, enrichment factor (EF), limit of quantification (LOQ), limit of detection (LOD), repeatability, and reproducibility. As shown in Table 2, a good linearity of response was observed in the range of 1.0–200  $\mu\text{g L}^{-1}$  for phoxim and fenitrothion, and in the range of 2.5–200  $\mu\text{g L}^{-1}$  for temephos, with a correlation coefficient of 0.9952–0.9990. LODs were found to be as low as 0.2–1.0  $\mu\text{g L}^{-1}$  for the three OPPs. EFs of the  $\text{ZrO}_2/\text{PDDA-GOA-SSM}$  for the three OPPs were evaluated, which were 20.0, 20.9, and 18.7, respectively. Five consecutive extractions using a single-extraction column were performed in the standard solution, and relative standard deviations (RSDs) were in the range of 1.3%–7.6%. The reproducibility was estimated through the recoveries of five different prepared SSMs for OPPs, and RSDs were in the range of 6.4%–10.1%. Thus, the established  $\text{ZrO}_2/\text{PDDA-GOA-SSM}$  possessed high-extraction recoveries as well as good repeatability.

Table 2. Analytical parameters for OPPs measured with the proposed  $\text{ZrO}_2/\text{PDDA-GOA-SSM-SPE-HPLC-UV}$  method.

Compound	Linear Equation	Linear Range ( $\mu\text{g L}^{-1}$ )	R <sup>a</sup>	EF <sup>b</sup>	LOQ <sup>c</sup> ( $\mu\text{g L}^{-1}$ )	LOD <sup>d</sup> ( $\mu\text{g L}^{-1}$ )	Repeatability (RSD <sup>e</sup> , n = 5, %)	Reproducibility (RSD, n = 5, %)
Phoxim	$y = 0.2329x + 0.2541$	1–200	0.9952	20.0	1	0.5	7.6	10.1
Temephos	$y = 0.2571x + 0.3962$	2.5–200	0.9964	20.9	2.5	1.0	1.3	8.5
Fenitrothion	$y = 0.1983x + 0.1864$	1–200	0.9990	18.7	1	0.2	5.0	6.4

<sup>a</sup> Correlation coefficient. <sup>b</sup> EF, enrichment factor. <sup>c</sup> LOQ, limit of quantification. <sup>d</sup> LOD, limit of detection for S/N = 3. <sup>e</sup> RSD, relative standard deviation.

### 3.6. Stability and Lifetime

The stability and lifetime of the sorbent are also important parameters for the practical application. The mechanical structure of the single GOA was unstable. When added with the PDDA, the GOA was not easy to drop from the surface of SSM. Figure S2 shows the change of extraction recoveries obtained by the proposed  $ZrO_2/PDDA-GOA-SSM$  after using it several times. After eight times, extraction recoveries decreased by about 5%–10%. This presented that the  $ZrO_2/PDDA-GOA-SSM$  was relative stable, which means it could meet the requirement. Therefore, in this experiment, a  $ZrO_2/PDDA-GOA-SSM$ -packed extraction column could be used eight times and then discarded.

### 3.7. Application in Real Sample

In order to verify the applicability of the  $ZrO_2/PDDA-GOA-SSM-SPE-HPLC-UV$  method, two vegetables (chives and pak choi) were analyzed. Generally, with the spraying of pesticides, leafy vegetables possess more residual pesticides, so pak choi and chives as two leafy vegetables that are commonly consumed were selected as the target samples to be detected and analyzed. Figure 7 shows typical chromatograms of the two vegetables and samples spiked with different concentrations of standard solutions. There was no analyte detected in the real samples. The applicability of this method was also evaluated by the matrix effect and relative recoveries of analytes. Three-level concentrations of the standard solution ( $20 \mu\text{g L}^{-1}$ ,  $40 \mu\text{g L}^{-1}$ ,  $100 \mu\text{g L}^{-1}$ ) were added into the samples to calculate the relative recovery. As shown in Table 3, the relative recoveries were in the range of 51.3%–92.7%. The matrix effect was calculated by the equation:  $ME (\%) = B/A \times 100$ , where A was the slope of calibration curve in the standard solution and B was the slope of calibration curve of OPPs in the real samples. The ME values of phoxim, temephos, and fenitrothion were 46.5%, 90.1%, and 82.1% for the pak choi, and 75.2%, 68.6%, and 72.4% for the chives, respectively. The low ME value of 46.5% was due to the low concentration of OPPs. Other ME values exhibited the matrix weakening effect in the sample analysis. The results also show that, compared with other environmental samples, the matrix effect in food samples was relatively obvious due to the complex interferences.

The established  $ZrO_2/PDDA-GOA-SSM-SPE-HPLC-UV$  method was compared with other reported methods with regard to the determination of OPPs. As listed in Table S1, most of the reported works mainly focused on liquid samples, and there were relatively less studies concerning vegetables as solid samples. Compared to the proposed method, this method demonstrated medium linear range and LODs. However, the LOD of this method ( $0.2 \mu\text{g L}^{-1}$ ,  $0.002 \text{ mg kg}^{-1}$ ) was lower than the maximum residue limit ( $0.2 \text{ mg kg}^{-1}$ ), which shows that it could meet the requirement for the limited detection of OPPs.

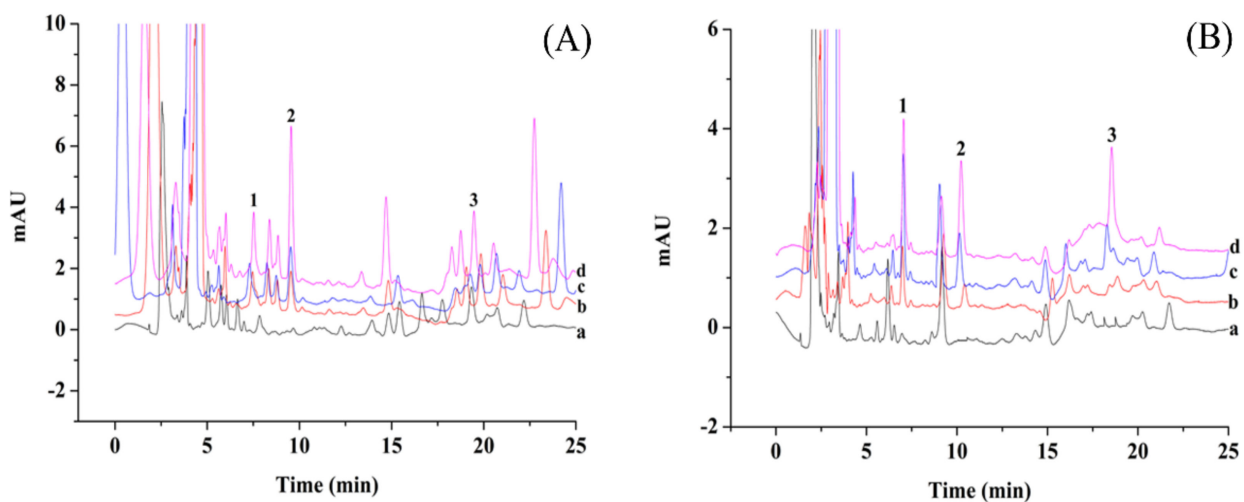


**Figure 7.** Chromatograms of pakvchoi (A) and chives (B), and samples (line a) spiked with standard solutions of  $20 \mu\text{g L}^{-1}$  (line b),  $40 \mu\text{g L}^{-1}$  (line c), and  $100 \mu\text{g L}^{-1}$  (line d) by the proposed method.

**Table 3.** Relative recoveries added with different concentrations of the standard solution in two vegetables.

Compound	Added ( $\mu\text{g g}^{-1}$ )	Pak Choi		Chives	
		Recovery (%)	RSD ( $n = 3$ , %)	Recovery (%)	RSD ( $n = 3$ , %)
Phoxim	20	51.3	1.2	67.0	4.4
	40	69.8	5.3	92.7	8.3
	100	52.5	0.6	80.6	15.0
Temephos	20	91.9	0.6	71.7	6.0
	40	83.5	2.9	86.2	2.9
	100	91.8	5.3	63.8	2.0
Fenitrothion	20	80.3	5.5	53.6	3.4
	40	81.9	4.9	66.9	2.7
	100	78.9	1.8	73.4	2.2

#### 4. Conclusions

In this research, a  $\text{ZrO}_2/\text{PDDA-GOA}$ -modified SSM was obtained through the chemical modification and freeze-drying, which was used for the extraction and determination of OPPs in vegetables. SSM, as a novel substrate, relatively reduced the accumulation of graphene. Compared with commercial extraction materials and other prepared materials (APTES-SSM,  $\text{ZrO}_2/\text{PDDA-GO-SSM}$ ), the  $\text{ZrO}_2/\text{PDDA-GOA}$ -modified SSM exhibited higher extraction recoveries for analytes. The excellent extraction efficiency of this sorbent was attributed to the unique properties of GOA, the selective adsorption of  $\text{ZrO}_2$  for OPPs, and the characteristic permeability of the SSM substrate. This indicates that the cheap and accessible SSM, as an important component of extraction devices, could be used in the following applications. The established  $\text{ZrO}_2/\text{PDDA-GOA-SSM}$  method could be successfully applied for the detection of OPPs in real samples, and this novel sorbent has been proved to be a promising candidate for the extraction of OPPs.

**Supplementary Materials:** The following are available online at <https://www.mdpi.com/article/10.3390/foods10071616/s1>, Figure S1. SEM images of the etched SSM, PDDA-GOA-coated SSM, and  $\text{ZrO}_2/\text{PDDA-GOA}$ -coated SSM. Figure S2: Evaluation of sorbent lifetime after using several times, Table S1: Comparison of methods used for the determination of OPPs.

**Author Contributions:** Conceptualization, X.H.; methodology, X.H.; software, X.H. and S.Y.; validation, R.D. and S.Y.; formal analysis, X.H. and H.Z.; investigation, R.D.; resources, X.H. and H.Z.; data curation, X.H. and R.D.; writing—original draft preparation, X.H.; writing—review and editing, W.W. and Q.Y.; visualization, W.W.; supervision, Q.Y.; project administration, Q.Y.; funding acquisition, X.H. All authors have read and agreed to the published version of the manuscript.

**Funding:** This research was funded by the National Natural Science Foundation of China, grant number 31901766, the Talents of High-Level Scientific Research Foundation, Qingdao Agricultural University, grant number 1119014, 1120023, and Breeding Plan of Shandong Provincial Qingchuang Research Team (2019).

**Conflicts of Interest:** The authors declare no conflict of interest. The funders had no role in the design of the study; in the collection, analyses, or interpretation of data; in the writing of the manuscript, or in the decision to publish the results.

#### References

- Teodoro, M.; Briguglio, G.; Fenga, C.; Costa, C. Genetic polymorphisms as determinants of pesticide toxicity: Recent advances. *Toxicol. Rep.* **2019**, *6*, 564–570. [[CrossRef](#)]
- Yang, F.W.; Li, J.W.; Pang, G.F.; Ren, F.Z.; Fang, B. Effects of diethyl phosphate, a non-specific metabolite of organophosphorus pesticides, on serum lipid, hormones, inflammation, and gut microbiota. *Molecules* **2019**, *24*, 2003. [[CrossRef](#)] [[PubMed](#)]
- Wang, J.W.; Teng, Y.G.; Zhang, C.X.; Liao, X.P.; Zhai, Y.Z.; Zuo, R. Activation of manganese dioxide with bisulfite for enhanced abiotic degradation of typical organophosphorus pesticides: Kinetics and transformation pathway. *Chemosphere* **2019**, *226*, 858–864. [[CrossRef](#)] [[PubMed](#)]



4. Huang, X.C.; Ma, J.K.; Feng, R.X.; Wei, S.L. Simultaneous determination of five organophosphorus pesticide residues in different food samples by solid-phase microextraction fibers coupled with high-performance liquid chromatography. *J. Sci. Food Agric.* **2019**, *99*, 6998–7007. [[CrossRef](#)] [[PubMed](#)]
5. Lu, D.K.; Liu, C.; Deng, J.K.; Zhou, X.G.; Shi, G.Y.; Zhou, T.S. Rational design of an ionic liquid dispersive liquid-liquid micro-extraction method for the detection of organophosphorus pesticides. *Analyst* **2019**, *144*, 2166–2172. [[CrossRef](#)] [[PubMed](#)]
6. González-Curbelo, M.Á.; Hernández-Borges, J.; Borges-Miquel, T.M.; Rodríguez-Delgado, M.Á. Determination of organophosphorus pesticides and metabolites in cereal-based baby foods and wheat flour by means of ultrasound-assisted extraction and hollow-fiber liquid-phase microextraction prior to gas chromatography with nitrogen phosphorus detection. *J. Chromatogr. A* **2013**, *1313*, 166–174. [[CrossRef](#)]
7. Kermani, M.; Jafari, M.T.; Saraji, M. Porous magnetized carbon sheet nanocomposites for dispersive solid-phase microextraction of organophosphorus pesticides prior to analysis by gas chromatography-ion mobility spectrometry. *Microchim. Acta* **2019**, *186*, 88. [[CrossRef](#)]
8. Zohrabi, P.; Shamsipur, M.; Hashemi, M.; Hashemi, B. Liquid-phase microextraction of organophosphorus pesticides using supramolecular solvent as a carrier for ferrofluid. *Talanta* **2016**, *160*, 340–346. [[CrossRef](#)]
9. Manafi Khoshmanesh, S.; Hamishehkar, H.; Razmi, H. Trace analysis of organophosphorus pesticide residues in fruit juices and vegetables by an electrochemically fabricated solid-phase microextraction fiber coated with a layer-by-layer graphenized graphite/graphene oxide/polyaniline nanocomposite. *Anal. Methods* **2020**, *12*, 3268–3276. [[CrossRef](#)] [[PubMed](#)]
10. Zeng, J.B.; Li, Y.L.; Zheng, X.F.; Li, Z.Z.; Zeng, T.; Duan, W.; Li, Q.; Shang, X.; Dong, B. Controllable transformation of aligned ZnO nanorods to ZIF-8 as solid-phase microextraction coatings with tunable porosity, polarity, and conductivity. *Anal. Chem.* **2019**, *91*, 5091–5097. [[CrossRef](#)]
11. Qin, P.G.; Zhu, W.L.; Han, L.Z.; Zhang, X.W.; Zhao, B.; Zhang, X.B.; Lu, M.H. Monodispersed mesoporous SiO<sub>2</sub>@metal-organic framework (MSN@MIL-101(Fe)) composites as sorbent for extraction and preconcentration of phytohormones prior to HPLC-DAD analysis. *Microchim. Acta* **2020**, *187*, 367. [[CrossRef](#)]
12. Lin, X.P.; Wang, X.Q.; Wang, J.; Yuan, Y.W.; Di, S.S.; Wang, Z.W.; Xu, H.; Zhao, H.Y.; Zhao, C.S.; Ding, W.; et al. Magnetic covalent organic framework as a solid-phase extraction absorbent for sensitive determination of trace organophosphorus pesticides in fatty milk. *J. Chromatogr. A* **2020**, *1627*, 461387. [[CrossRef](#)] [[PubMed](#)]
13. Du, L.Y.; Wang, X.D.; Liu, T.T.; Li, J.Y.; Wang, J.X.; Gao, M.; Wang, H.L. Magnetic solid-phase extraction of organophosphorus pesticides from fruit juices using NiFe<sub>2</sub>O<sub>4</sub>@polydopamine/Mg/Al-layered double hydroxides nanocomposites as an adsorbent. *Microchem. J.* **2019**, *150*, 104128. [[CrossRef](#)]
14. Mehdipour, M.; Ansari, M.; Pournamdari, M.; Zeidabadinejad, L.; Kazemipour, M. Selective extraction of malathion from biological fluids by molecularly imprinted polymer coated on spinel ZnFe<sub>2</sub>O<sub>4</sub> magnetic nanoparticles based on green synthesis. *Sep. Sci. Technol.* **2020**, *56*, 1899–1909. [[CrossRef](#)]
15. Zhang, J.; Li, W.Q.; Zhu, W.L.; Yang, Y.X.; Qin, P.G.; Zhou, Q.; Lu, M.H.; Cai, Z.W. Mesoporous graphitic carbon nitride as an efficient sorbent for extraction of sulfonamides prior to HPLC analysis. *Microchim. Acta* **2019**, *186*, 279. [[CrossRef](#)] [[PubMed](#)]
16. Yang, Y.X.; Qin, P.G.; Zhang, J.; Li, W.Q.; Zhu, J.H.; Lu, M.H.; Cai, Z.W. Fabrication of nanoscale graphitic carbon nitride/copper oxide hybrid composites coated solid-phase microextraction fibers coupled with gas chromatography for determination of polycyclic aromatic hydrocarbons. *J. Chromatogr. A* **2018**, *1570*, 47–55. [[CrossRef](#)] [[PubMed](#)]
17. Feng, J.J.; Loussala, H.M.; Han, S.; Ji, X.P.; Li, C.Y.; Sun, M. Recent advances of ionic liquids in sample preparation. *TrAC Trends Anal. Chem.* **2020**, *125*, 115833. [[CrossRef](#)]
18. Tian, Y.; Feng, J.J.; Wang, X.Q.; Luo, C.N.; Sun, M. Ionic liquid-functionalized silica aerogel as coating for solid-phase microextraction. *J. Chromatogr. A* **2019**, *1583*, 48–54. [[CrossRef](#)]
19. Feng, J.J.; Wang, X.Q.; Han, S.; Ji, X.P.; Li, C.Y.; Luo, C.N.; Sun, M. An ionic-liquid-modified melamine-formaldehyde aerogel for in-tube solid-phase microextraction of estrogens followed by high performance liquid chromatography with diode array detection. *Microchim. Acta* **2019**, *186*, 769. [[CrossRef](#)]
20. Amiri, A.; Ghaemi, F. Graphene grown on stainless steel mesh as a highly efficient sorbent for sorptive microextraction of polycyclic aromatic hydrocarbons from water samples. *Anal. Chim. Acta* **2017**, *994*, 29–37. [[CrossRef](#)]
21. Hu, H.; Zhao, Z.B.; Wan, W.B.; Gogotsi, Y.; Qiu, J.S. Ultralight and highly compressible graphene aerogels. *Adv. Mater.* **2013**, *25*, 2219–2223. [[CrossRef](#)]
22. Zhao, J.; Zhang, Y.Z.; Chen, J.Y.; Zhang, W.L.; Yuan, D.; Chua, R.; Alshareef, H.N.; Ma, Y.W. Codoped holey graphene aerogel by selective etching for high-performance sodium-ion storage. *Adv. Energy Mater.* **2020**, *10*, 2000099. [[CrossRef](#)]
23. Han, Q.; Yang, L.; Liang, Q.L.; Ding, M.Y. Three-dimensional hierarchical porous graphene aerogel for efficient adsorption and preconcentration of chemical warfare agents. *Carbon* **2017**, *122*, 556–563. [[CrossRef](#)]
24. Tang, S.; Sun, J.; Xia, D.; Zang, B.; Gao, Y.; Chen, C.; Shen, W.; Lee, H.K. In-syringe extraction using compressible and self-recoverable, amphiphilic graphene aerogel as sorbent for determination of phenols. *Talanta* **2019**, *195*, 165–172. [[CrossRef](#)] [[PubMed](#)]
25. Wu, Q.; Wu, W.; Zhan, X.; Hou, X.D. Three-dimensional chitosan/graphene oxide aerogel for high-efficiency solid-phase extraction of acidic herbicides in vegetables. *New J. Chem.* **2020**, *44*, 10654–10661. [[CrossRef](#)]
26. Zhao, M.H.; Reda, A.T.; Zhang, D.X. Reduced graphene oxide/ZIF-67 aerogel composite material for uranium adsorption in aqueous solutions. *ACS Omega* **2020**, *5*, 8012–8022. [[CrossRef](#)]



27. Sharma, B.; Thakur, S.; Trache, D.; Nezhad, H.Y.; Thakur, V.K. Microwave-assisted rapid synthesis of reduced graphene oxide-based gum tragacanth hydrogel nanocomposite for heavy metal ions adsorption. *Nanomaterials* **2020**, *10*, 1616. [[CrossRef](#)] [[PubMed](#)]
28. Arabkhani, P.; Asfaram, A. Development of a novel three-dimensional magnetic polymer aerogel as an efficient adsorbent for malachite green removal. *J. Hazard. Mater.* **2020**, *384*, 121394. [[CrossRef](#)]
29. Huangfu, Y.M.; Ruan, K.P.; Qiu, H.; Lu, Y.J.; Liang, C.B.; Kong, J.; Gu, J.W. Fabrication and investigation on the PANI/MWCNT/thermally annealed graphene aerogel/epoxy electromagnetic interference shielding nanocomposites. *Compos. Part A Sci. Manuf.* **2019**, *121*, 265–272. [[CrossRef](#)]
30. Bai, R.X.; Yang, F.; Meng, L.Y.; Zhao, Z.G.; Guo, W.H.; Cai, C.Q.; Zhang, Y. Polyethylenimine functionalized and scaffolded graphene aerogel and the application in the highly selective separation of thorium from rare earth. *Mater. Des.* **2021**, *197*, 109195. [[CrossRef](#)]
31. Hou, X.D.; Yu, H.; Yan, S.H.; Xiao, J.X.; Sun, M.; Wu, W. Cationic polyelectrolyte/graphene oxide as an efficient sorbent for the extraction and analysis of trace acidic herbicides in vegetables. *J. Chromatogr. A* **2020**, *1618*, 460884. [[CrossRef](#)]
32. Tong, Z.B.; Xu, M.Q.; Li, Q.; Liu, C.; Wang, Y.L.; Sha, J.Q. Polyelectrolyte-functionalized reduced graphene oxide wrapped helical POMOF nanocomposites for bioenzyme-free colorimetric biosensing. *Talanta* **2020**, *220*, 121373. [[CrossRef](#)]
33. Tian, J.M.; Mu, Z.D.; Wang, J.; Zhou, J.; Yuan, Y.H.; Bai, L.J. Electrochemical aptasensor for ultrasensitive detection of lipopolysaccharide using silver nanoparticles decorated titanium dioxide nanotube/functionalized reduced graphene oxide as a new redox nanoprobe. *Microchim. Acta* **2021**, *188*, 31. [[CrossRef](#)] [[PubMed](#)]
34. Rahbar, N.; Behrouz, E.; Ramezani, Z. One-step synthesis of zirconia and magnetite nanocomposite immobilized chitosan for micro-solid-phase extraction of organophosphorous pesticides from juice and water samples prior to gas chromatography/mass spectroscopy. *Food Anal. Method* **2017**, *10*, 2229–2240. [[CrossRef](#)]
35. Kweon, H.K.; Håkansson, K. Selective zirconium dioxide-based enrichment of phosphorylated peptides for mass spectrometric analysis. *Anal. Chem.* **2006**, *78*, 1743–1749. [[CrossRef](#)] [[PubMed](#)]
36. Liu, A.J.; Kou, W.; Zhang, H.; Xu, J.Q.; Zhu, L.X.; Kuang, S.L.; Huang, K.K.; Chen, H.W.; Jia, Q. Quantification of trace organophosphorus pesticides in environmental water via enrichment by magnetic-zirconia nanocomposites and online extractive electrospray ionization mass spectrometry. *Anal. Chem.* **2020**, *92*, 4137–4145. [[CrossRef](#)]
37. Gannavarapu, K.P.; Ganesh, V.; Thakkar, M.; Mitra, S.; Dandamudi, R.B. Nanostructured diatom-ZrO<sub>2</sub> composite as a selective and highly sensitive enzyme free electrochemical sensor for detection of methyl parathion. *Sens. Actuators B Chem.* **2019**, *288*, 611–617. [[CrossRef](#)] [[PubMed](#)]
38. Zare, M.; Ramezani, Z.; Rahbar, N. Development of zirconia nanoparticles-decorated calcium alginate hydrogel fibers for extraction of organophosphorous pesticides from water and juice samples: Facile synthesis and application with elimination of matrix effects. *J. Chromatogr. A* **2016**, *1473*, 28–37. [[CrossRef](#)]
39. Hou, X.D.; Liu, S.J.; Zhou, P.P.; Li, J.; Liu, X.; Wang, L.C.; Guo, Y. Polymeric ionic liquid modified graphene oxide-grafted silica for solid-phase extraction to analyze the excretion-dynamics of flavonoids in urine by Box-Behnken statistical design. *J. Chromatogr. A* **2016**, *1456*, 10–18. [[CrossRef](#)]